

MICROSTRUCTURE EVOLUTION AND MECHANICAL PROPERTIES DEGRADATION OF HPNB ALLOY AFTER AN ELEVEN-YEAR SERVICE

MIKROSTRUKTURNI RAZVOJ I DEGRADACIJA MEHANIČKIH SVOJSTAVA LEGURE HPNB POSLE JEDANAEST GODINA EKSPLOATACIJE

Originalni naučni rad / Original scientific paper
UDK /UDC:

Rad primljen / Paper received: 25.08.2022

Adresa autora / Author's address:

¹) University of Kragujevac, Faculty of Mechanical and Civil Engineering in Kraljevo, Kraljevo, Serbia

²) University of Belgrade, Innovation Centre of the Faculty of Mechanical Engineering, Belgrade, Serbia

*email: olivera66eric@gmail.com

³) University of Novi Sad, Faculty of Technical Science, Novi Sad, Serbia

⁴) University of Belgrade, Faculty of Technology and Metallurgy, Belgrade, Serbia

Keywords

- HP40Nb alloy
- microstructure
- fracture mode
- carbide phases

Abstract

In this work, the heat-resistant cast steel HP40Nb alloy, produced in the form of a centrifugally cast tube, which failed after 11.4 years service is investigated. The microstructure is examined using a scanning electron microscope (SEM), while the phases observed are analysed using an energy dispersive X-ray analyser system (EDS). Additionally, fractography is performed on the fractured surface of failed specimens. Mechanical properties of the tube are evaluated by using tensile and Charpy impact testing at room temperature (298 K). Main results indicate that the failed tube microstructure consists of an austenitic matrix and a continuous network of primary eutectic carbides of two types: one rich in Nb (bright particles), and one rich in Cr (dark particles). These carbides are NbC and complex M_7C_3 ($M = Cr, Ni, Fe$) type. The brittle intergranular fracture mode is explained by the presence of massive precipitation and coarsening of intergranular carbides at grain boundaries. Lower tensile properties of the in-service exposed tube might be correlated to the morphological, chemical, and distribution changes of precipitates during service at high temperature. Decreased values of hardness can be attributed to increase in grain size, as well as due to the decomposition of Cr-carbide during the heat treatment at temperatures above 1073 K.

INTRODUCTION

The conventional industrial process for producing ethylene is supported by the pyrolysis of a mixture of hydrocarbons in a pyrolysis furnace at temperature ranges from 1173 to 1373 K, /1/. The heat-resisting (H-series) centrifugally cast austenitic stainless steels are typically used for pyrolysis tubes. A unique combination of their superior temperature, creep strength, good oxidation and carburization resistance makes heat-resistant cast steel HPNb alloys suitable to be used in cracking furnaces, /2, 3/.

Ključne reči

- HP40Nb legura
- mikrostruktura
- morfologija loma
- karbidne faze

Izvod

U ovom radu je ispitivana legura od livenog čelika HP40Nb otpornog na toplotu, proizvedena u obliku centrifugalno livene cevi, koja je otkazala posle 11,4 godina eksploatacije. Mikrostruktura je ispitivana primenom skenirajućeg elektronskog mikroskopa SEM, dok su uočene faze analizirane korišćenjem sistema energetske disperzivnog rendgenskog analizatora (EDS). Dodatno, fraktografija je urađena na površini loma oštećenih uzoraka. Mehanička svojstva su procenjena ispitivanjem na zatezanje i ispitivanjem energije udara po Šarpiju na sobnoj temperaturi (298 K). Glavni rezultati su pokazali da se mikrostruktura oštećene cevi sastoji od austenitne osnove i neprekidne mreže primarnih eutektičkih karbida dva tipa: jednog bogatog Nb (svetle čestice) i jednog bogatog Cr (tamne čestice). Oba karbida su tipa NbC i složeni M_7C_3 ($M = Cr, Ni, Fe$). Mehanizam krtog intergranularnog loma objašnjen je prisustvom masivnog taloženja grubih intergranularnih karbida na granicama zrna. Niža zatezna svojstva cevi izložene eksploataciji mogu biti u korelaciji sa morfološkim, hemijskim i distributivnim promenama taloga tokom eksploatacije na visokoj temperaturi. Smanjenje vrednosti tvrdoće može se pripisati povećanju veličine zrna kao i razlaganju Cr-karbida tokom termičke obrade na temperaturama iznad 1073 K.

The ethylene cracking tube is an important section of a petrochemical plant. These parts are generally designed for a normal lifetime of 100,000 h of service at an operating temperature of 1173 K. However, their design life, which varies from 30,000 to 180,000 h, is not expected to be equal to the actual life depending on real operating conditions /4/. The premature failures of furnace columns are frequently observed as a result of a number of damage mechanisms, such as creep, carburization, oxidation, thermal shock, and accidental overheating, /4-13/.

An overview of the literature indicates that tube failure caused by carbonization accounts for 49 % of the total failed tubes, /14/. Thus, a large number of studies have been published on the detection of carburized tubes /2, 3/, fracture analysis /7, 15/, carbonization mechanism /16, 17/, and microstructure analysis of carburization layer /18, 19/. Degradation of microstructural and mechanical properties of tube materials is an important performance factor determined by the accumulation of this damage and could rapidly develop into fatal rupture of tubes, especially when overheating, thermal shock, or unplanned shutdown, /7, 20-22/.

Having all this in mind, the aim of the present research is focused on the investigation of material degradation through microstructural and mechanical characterization of microalloyed HP40Nb heat-resistant stainless steel tube, which has failed after 11.4 years in service.

EXPERIMENTS

Material and methods

The material used in this study is a centrifugal cast austenitic HP40Nb grade alloy. The sections of the tube are taken out of the service after 100,000 h (the failed tube). All samples are cut from HP40Nb radiant tube in an ethylene cracking unit after service. The exact locations where the sections are cut on the reformer columns in the respective plants are unknown precisely. Tube segments of 350 mm in length, are cut from the furnace regions which have been in exploitation for 11.4 years. Operating condition of the tubes is at 1143 K (870 °C) under maximum internal pressure of 2.5 bars (250 kPa).

The chemical composition of the service reformer tube is analysed through standard analytical spectrometry method, using the Optical Energy Spectrometer (OES) type I Spark 8860, Thermo Scientific™, USA.

Metallographic specimens are prepared in accordance with standard metallographic preparation technique: grinding (with SiC papers, from 180 to 2400), polishing (diamond suspensions with 6, 3, 1 and 1/4 µm particle size) and etched with a solution of 15 ml HCl, 10 ml Glycerol, and 5 ml HNO₃.

The microstructure is examined using scanning electron microscope JOEL JSM 6460 LV. The phases observed are analysed using an energy dispersive X-ray analyser system (EDS) INCA Oxford Instruments in conjunction with a SEM. Fractography is performed on the fracture surface of failed specimens.

Mechanical properties of the tube are evaluated by using tensile testing and Charpy impact testing at room temperature (298 K). The tensile test of standard specimens (ISO 6892-1:2019) with a gauge length of 50 mm are carried out at room temperature using universal testing machine Schenck Trebel (1000 kN) under the constant cross head speed mode with a nominal strain rate of 2 mm/min.

Specimens for Sharp impact tests are 10×10×55 mm with 2 mm length 45° V notch of root radius 0.25 mm. The Brinell hardness of each tube samples is measured by universal hardness tester model Dia Testor 2Rc-S3-E, Otto Wolpert, according to the related ISO 6507-1 standard.

The X-ray phase analysis is performed with the help of a Rigaku Smartlab powder diffractometer. Radiation from the

copper anticathode with a wavelength of CuK = 0.154178 nm was used. The operating voltage on the tube was U = 40 kV, and the current I = 30 mA. The samples are examined under the following experimental conditions: range of diffraction angles 5-130° 2θ with a step of 0.01° and recording speed 6°/minute. Diffraction data are processed using the software package PDXL2 (version 2.8.30, Rigaku Co.). The position of the diffraction maxima (2θ), as well as the corresponding intensities (cps), are shown graphically. On the basis of the obtained values, by comparing with literature data and PDF standards, the present (only) crystalline phases whose content in the sample is greater than approximately 1 %, are identified.

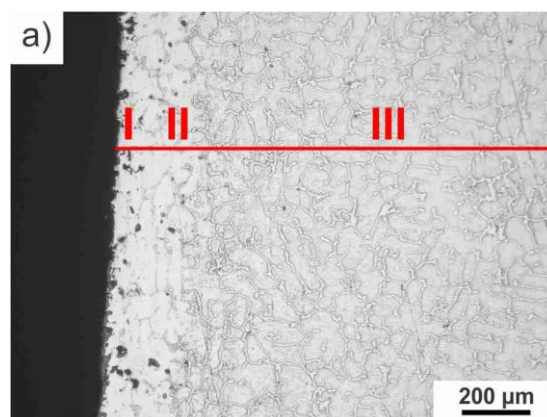
RESULTS AND DISCUSSION

Chemical composition

Chemical composition of the investigated alloy consists of: 0.45 % C; 0.97 % Mn; 1.36 % Si; 0.045 % P; 32.21 % Ni; 26.22 % Cr, and 1.5 % Nb (mass %).

Microstructural analysis

Microstructures of the ex-service material are shown in Fig. 1a-c. It can be seen that there are different microstructures in the exposed areas (the inner, outer surfaces, and central regions). A black phase (I in the micrograph Fig. 1a) is an oxide layer with thickness of about 30 µm. Closer to the inner surface (II in Fig. 1a), is a second zone prolonged for about 150 µm, showing the precipitate - free layer. According to Fig. 1a, the farthest from the inner wall side is the III zone. This zone has skeletal-shaped carbides and some secondary carbides within the austenitic matrix. According to Fig. 1b the material in the middle section consists of an austenitic dendritic matrix and a complex network of coarsened intergranular precipitates. Figure 1c shows typical damage to the outer surface of the radiant tubes. Unlike the tube's inner wall, the material degradation on the outer surface is different. Creep damage seems to be the main cause of material degradation in the tube outer wall as indicated by the formation of cavities which nucleate along grain boundaries, as seen in Fig. 1c. Some cavities which appear along dendritic boundaries, had already coalesced with each other, forming intergranular cracks at grain boundaries, thus indicating creep damage accumulation in the failed tube during long term service at high temperature, /23/.



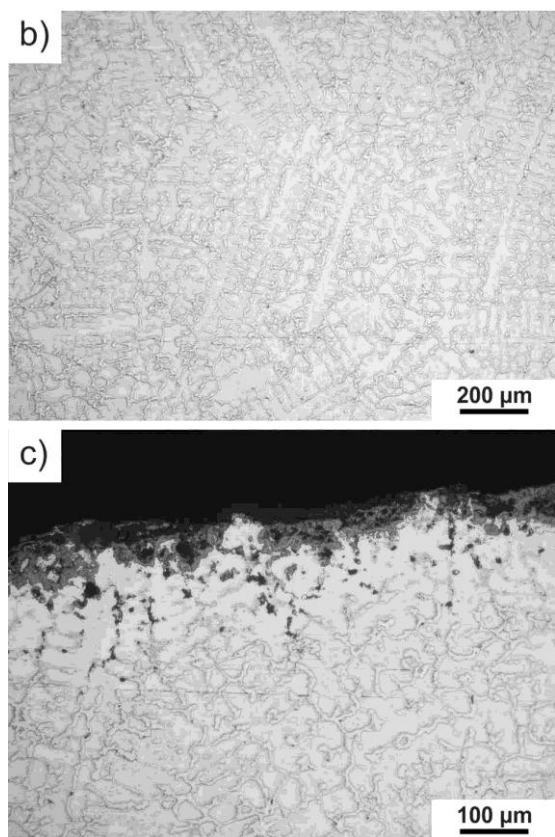


Figure 1. LM micrographs of sample cross sections from the tube close to the: a) inner surface; b) middle thickness; c) outer surface.

SEM micrograph of a carburized tube shows the outer scale, a precipitate free zone with micro-cracking, and carbide formation at the inside of the tube (Fig. 2).

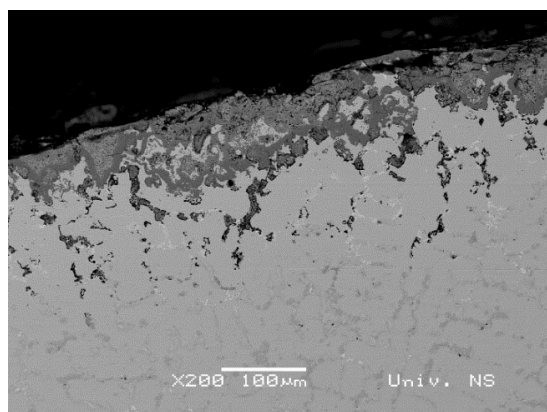


Figure 2. SEM micrograph at the inner section part of tube using backscattered electrons.

The precipitation of carbides can be identified to be of the two types as revealed in the SEM micrographs (Fig. 3a). Light grey ones are more continuous and plate-like, while the dark grey are present mostly at intra-dendritic locations, as confirmed by SEM-EDX studies (Table 1). The microstructure consists of an austenitic matrix (Spec 7) and a continuous network of primary eutectic carbides of two types: one rich in Nb (bright particles in Fig. 3b, Spec 3, 4, 5), and one rich in Cr (dark particles in Fig. 3b, Spec 2, 6). These carbides are NbC and complex M_7C_3 ($M = Cr, Ni, Fe$) type.

Carbides in the intra-dendritic boundaries appear as lamellar, or skeleton form, /23/. The niobium-rich carbides are more stable at high temperature compared to the secondary chromium carbides, /24/.

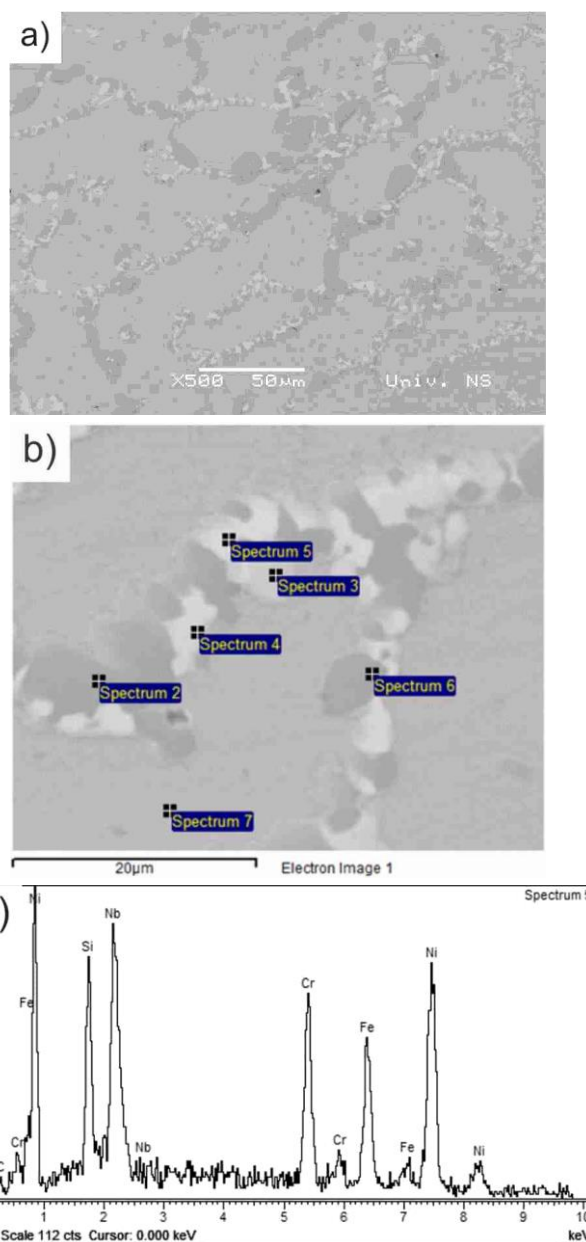


Figure 3. SEM and EDS analysis: a) SEM micrograph from cross section of the failed tube (11.4 years service) close to the inner surface; b) positions of EDS analysis (dark and light phases); c) corresponding EDS spectrum 5.

Table 1. Chemical composition (mass. %) of participate phases in HP40Nb alloy, corresponding to Fig. 3b.

	C	Si	Cr	Mn	Fe	Ni	Nb
Sum spectrum	4.06	2.06	27.64	1-01	30.98	30.17	4.08
Spectrum 2	9.42		52.79		20.90	16.89	
Spectrum 3	6.58	7.38	25.23		4.73	29.47	26.62
Spectrum 4	5.44	8.61	7.76		11.78	41.14	25.27
Spectrum 5	5.76	7.82	14.27		15.44	36.67	20.04
Spectrum 6	5.15	1.18	32.50	1.23	33.12	26.82	
Spectrum 7	3.64	1.18	20.36	1.32	39.60	33.89	

XRD analysis

In the failed tube sample the following crystal phases are identified: γ -Fe whose diffraction pattern corresponds to the standard PDF # 01-081-8770; Cr_{23}C_6 whose diffraction pattern corresponds to the standard PDF # 03-065-3132; Cr_7C_3 whose diffraction pattern corresponds to the standard PDF # 01-071-3789; $\text{Nb}_3\text{Ni}_2\text{Si}$ whose diffraction pattern corre-

sponds to standard PDF # 01-072-2171 (PDF-2 Release 2016 RDB), Fig. 4. Results of the submitted chemical analysis indicate the possibility of multiple atomic replacements in the mentioned crystal structures. The stated formulas of crystal phases should be considered as approximate chemical formulas.

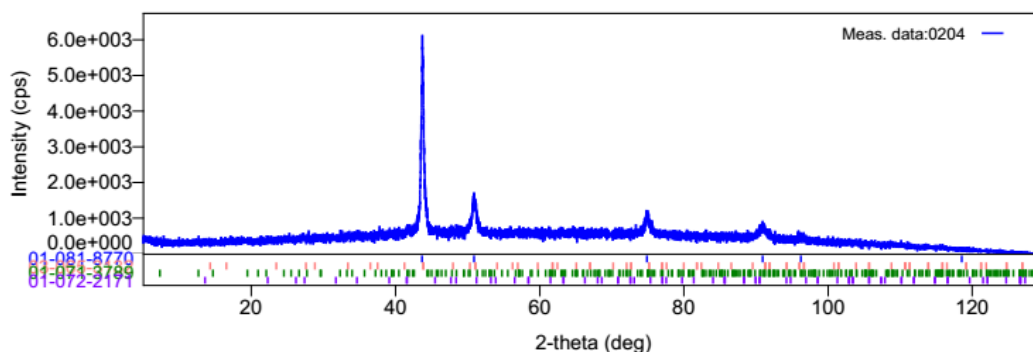


Figure 4. XRD patterns of the used tube are shown in blue.

In the lower part of the graphic, vertical lines show the reflection positions of the standards of the above-mentioned crystal types (taken from the PDF database) and numbers of corresponding cards. The first row shows reflection positions of γ -Fe in blue, the second row shows reflection positions of M_{23}C_6 in pink, the third row shows reflection positions of M_7C_3 in green, and the fourth row shows the reflection positions of $\text{Nb}_3\text{Ni}_2\text{Si}$ in lilac.

Mechanical properties

Tensile and Charpy impact tests of the tube exposed in service at room temperature are shown in Table 2. As can be seen from this table, mechanical strength (proof strength and tensile strength) and elongation of the service exposed tube have decreased compared the as-cast tube. Lower tensile properties of the service exposed tube might be correlated to the morphological, chemical, and distribution changes of precipitates during service at high temperature, /25/.

The hardness of the service exposed tube is 185 HB. The decreased values of hardness can be attributed to increase in grain size, as well as due to decomposition of Cr-carbide during heat treatment at temperatures above 1073 K, /26/.

Table 2. Mechanical properties of HP40Nb alloy.

Sample	Tensile test			Hardness HB	Charpy impact test Impact energy (J)
	R_m (MPa)	$R_{p0.2}$ (MPa)	A (%)		
As cast tube	450	240	10	215	-
Service exposed tube	358	308	4.5	185	4.4

Fractography

To verify the observed differences in fracture behaviour, the fractured surfaces of tensile and impact test specimens are examined using SEM. This investigation reveals that both types of microstructures show very similar fracture morphology (Figs. 5 and 6). The brittle mechanism of fracture predominates on fractured surfaces, although some other

modes are also present. The brittle intergranular fracture mode is explained by the presence of massive precipitation and coarsening of intergranular carbides at grain boundaries (Fig. 5). These precipitates have been brittle and have produced secondary cracks, which significantly decrease grain-boundary strength and toughness of tube material, /22, 26, 27/.

Morphological features that appeared in the failed specimen after Charpy impact test illustrate a signature of the brittle mode of fracture. The presence of microcracks and microvoids act as initiation sites and provide an easy way for the crack to propagate during the Charpy impact test and ultimately lowering the fracture toughness of this material. Low-magnification observation (Fig. 6a) of the fractured surface of the specimen tested at room temperature reveals quasi-cleavage features. The figure shows a number of large voids like features on the fractured surface. As can be seen in Fig. 6b, the high magnification reveals intergranular cleavage features and microcracks on the fractured surface, indicating the dominant failure mechanism as brittle fracture.

CONCLUSIONS

In this study, the microalloyed HP40Nb heat-resistant stainless steel tube, which failed after 11.4 years in service was investigated. The paper analyses the changes in microstructure and mechanical properties which occurred in service after operation at elevated temperatures for more than 100,000 hours.

The conclusions of the research are:

- The microstructure of HP40Nb alloy in the as-cast condition, from which the pyrolysis tube is made of, consists of an austenitic base in the form of a dendrite structure containing a network of skeletons of primary eutectic carbides of the MC type, rich in Nb, and of the M_{23}C_6 type, rich in Cr precipitated at grain boundaries.
- After a long time of operation of the HP40Nb alloy pipes at high temperatures, the mechanical properties of the tested material are degraded which is correlated with the change in the type, quantity, and morphology of the precipitated intermetallic phases.

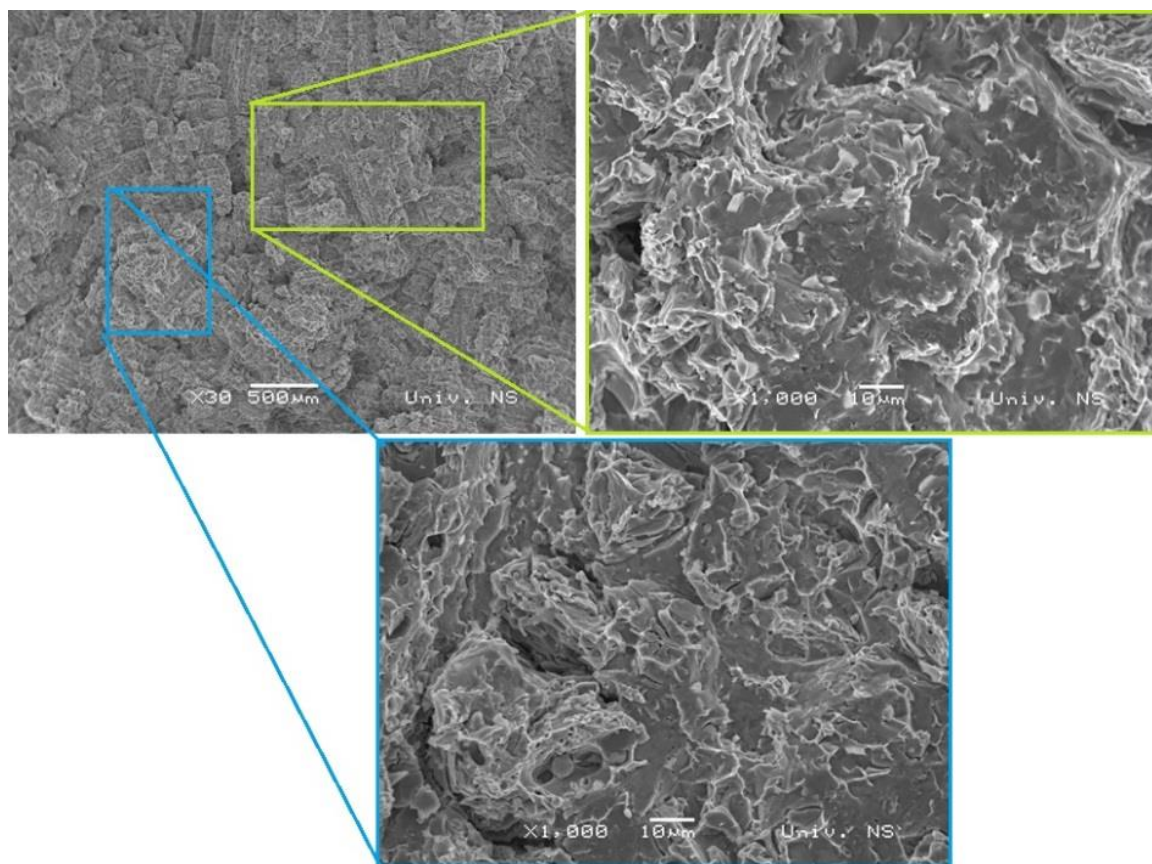


Figure 5. Fractography of the HP40Nb alloy specimen at different magnifications after the tensile test.

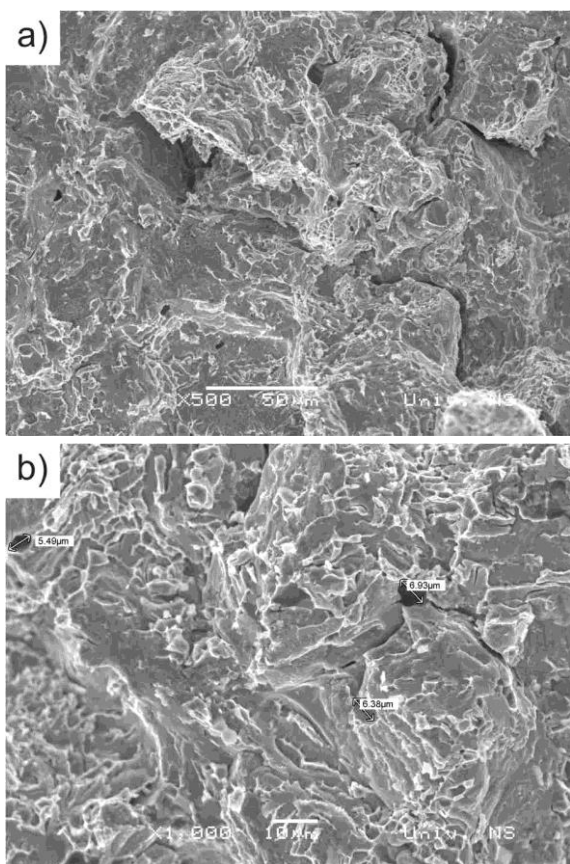


Figure 6. Fracture surfaces of Charpy impact specimens of HP40Nb alloys after service.

ACKNOWLEDGEMENTS

This work is supported by the Serbian Ministry for Education, Science and Technological Development by contracts No. 451-03-68/2022-14/200108, 451-03-68/2022-16/200156, No. 451-03-68/2022-14/200213, and No. 451-03-68/2022-14/200135.

REFERENCES

1. Wang, W.Z., Xuan, F.Z., Wang, Z.D., et al. (2011), *Effect of overheating temperature on the microstructure and creep behavior of HP40Nb alloy*, Mater. Des. 32(7): 4010-4016. doi: 10.1016/j.matdes.2011.03.008
2. Allahkaram, S.R., Borjali, S., Khosravi, H. (2012), *Investigation of weldability and property changes of high pressure heat-resistant cast stainless steel tubes used in pyrolysis furnaces after a five-year service*, Mater. Des. 33: 476-484. doi: 10.1016/j.matdes.2011.04.052
3. Shen, L.M., Gong, J.M., Jiang, Y., Geng, L.Y. (2011), *Effects of aging treatment on microstructure and mechanical properties of Cr25Ni35Nb and Cr35Ni45Nb furnace tube steel*, Acta Metall. Sin. - Engl. Lett. 24(3): 235-242. doi: 10.11890/1006-7191-113-235
4. Schillmoller, C.M. (1986), *Solving high-temperature problems in oil refineries and petrochemical plants*, Chem. Eng. 93(1): 83-87.
5. Gommans, R.J. (2002), *Life assessment and inspection techniques in reformer furnaces*, 6th Schmidt + Clemens group symposium, Bali Indonesia, 2002.
6. Shariat, M.H., Faraji, A.H., Ashraf-Riahy, A., Alipour, M.M. (2003), *In advanced creep failure of HP modified reformer tubes in an ammonia plant*, J Corros. Sci. Eng. 6. Paper H012 preprint 69.

7. Ul-Hamid, A., Tawancy, H.M., Mohamed, A.R.I., Abbas, N.M. (2006), *Failure analysis of furnace radiant tubes exposed to excessive temperature*, Eng. Fail. Anal. 13(6): 1005-1021. doi: 10.1016/j.engfailanal.2005.04.003
8. Yoon, K.B., Jeong, D.G. (1999), *Oxidation failure of radiant heater tubes*, Eng. Fail. Anal. 6(2): 101-112. doi: 10.1016/S1350-6307(98)00033-8
9. Guan, K., Xu, H., Wang, Z. (2005), *Analysis of failed ethylene cracking tubes*, Eng. Fail. Anal. 12(3): 420-431. doi: 10.1016/j.engfailanal.2004.03.012
10. Ferreira, H. (1997), *Investigation of an unusual reformer tube failure*, IMTOF 97.
11. Ghanem, M.M., Elbatahgy, A.-M. (2003), *Catastrophic failure of liquefied ammonia gas cylinder*, Mater. Perform. 42(4): 52-55.
12. Da Silveira, T.L., May, I.L. (2006), *Reformer furnaces: Materials, damage mechanisms and assessment*, Arabian J Sci. Eng. Sec. B: Eng. 31(2C): 99-119.
13. Swaminathan, J., Guguloth, K., Gunjan, M. (2008), *Failure analysis and remaining life assessment of service exposed primary reformer heater tubes*, Eng. Fail. Anal. 15(4): 311-331. doi: 10.1016/j.engfailanal.2007.02.004
14. Shen, L.M., Gong, J.M., Jiang, Y., Geng, L.Y. (2011), *Effects of aging treatment on microstructure and mechanical properties of Cr25Ni35Nb and Cr35Ni45Nb furnace tube steel*, Acta Metall. Sin. (Eng. Lett.), 24(3): 235-242. doi: 10.11890/1006-7191-113-235
15. Klöwer, J., Heubner, U. (1998), *Carburisation of nickel-base alloys and its effects on the mechanical properties*, Mater. Corros. 49(4): 237-245. doi: 10.1002/(SICI)1521-4176(199804)49:4<237::AID-MACO237>3.0.CO;2-5
16. Wu, X.Q., Jing, H.M., Zheng, Y.G., et al. (2001), *Coking of HP tubes in ethylene steam cracking plant and its mitigation*, Brit. Corros. J. 36(2): 121-126. doi: 10.1179/000705901101501541
17. Ramanarayanan, T.A., Petkovic, R.A., Mumford, J.D., Ozekcin, A. (1998), *Carburization of high chromium alloys*, Mater. Corros. 49(4): 226-230. doi: 10.1002/(SICI)1521-4176(199804)49:4<226::AID-MACO226>3.0.CO;2-D
18. Kaya, A.A. (2002), *Microstructure of HK40 alloy after high-temperature service in oxidizing/carburizing environment: II. Carburization and carbide transformations*, Mater. Charact. 49(1): 23-34. doi: 10.1016/S1044-5803(02)00284-X
19. Nishiyama, Y., Otsuka, N., Nishizawa, T. (2003), *Carburization resistance of austenitic alloys in CH₄-CO₂-H₂ gas mixtures at elevated temperatures*, Corrosion, 59(8): 688-700. doi: 10.5006/1.3277598
20. Guan, K., Wang, Q. (2011), *Analysis of failed electron beam welds in ethylene cracking tubes*, Eng. Fail. Anal. 18(5): 1366-1374. doi: 10.1016/j.engfailanal.2011.04.003
21. Tawancy, H.M. (2009), *Degradation of mechanical strength of pyrolysis furnace tubes by high-temperature carburization in a petrochemical plant*, Eng. Fail. Anal. 16(7): 2171-2178. doi: 10.1016/j.engfailanal.2009.02.009
22. Khodamorad, S.H., Haghshenas Fatmehsari, D., Rezaie, H., Sadeghipour, A. (2012), *Analysis of ethylene cracking furnace tubes*, Eng. Fail. Anal. 21: 1-8. doi: 10.1016/j.engfailanal.2011.11.018
23. Lee, J.H., Yang, W.J., Yoo, W.D., Cho, K.S. (2009), *Microstructural and mechanical property changes in HK40 reformer tubes after long term use*, Eng. Fail. Anal. 16(6): 1883-1888. doi: 10.1016/j.engfailanal.2008.09.032
24. Guguloth, K., Swaminathan, J., Bagui, S., Ray, A.K. (2012), *Remnant life assessment and microstructural studies on service exposed primary reformer tubes of a catalytic converter of an ammonia plant*, High Temp. Mater. Proc. 31(6): 759-767. doi: 10.1515/htmp-2012-0016
25. Aichaoui, M., Hadji, A. (2018), *Failure of service exposed heat resistant cast steel tube*, Int. J. Eng. Res. Africa, 34: 1-4. doi: 10.4028/www.scientific.net/JERA.34.1
26. Han, Z., Xie, G., Cao, L., et al. (2019), *Material degradation and embrittlement evaluation of ethylene cracking furnace tubes after long term service*, Eng. Fail. Anal. 97: 568-578. doi: 10.1016/j.engfailanal.2019.01.041
27. Ghatak, A., Robi, P.S. (2015), *High-temperature deformation behavior of HP40Nb micro-alloyed reformer steel*, Metall. Microstruct. Anal. 4(6): 508-517. doi: 10.1007/s13632-015-0235-z

© 2022 The Author. Structural Integrity and Life, Published by DIVK (The Society for Structural Integrity and Life 'Prof. Dr Stojan Sedmak') (<http://divk.inovacionicentar.rs/ivk/home.html>). This is an open access article distributed under the terms and conditions of the [Creative Commons Attribution-NonCommercial-NoDerivatives 4.0 International License](https://creativecommons.org/licenses/by-nc-nd/4.0/)